

Characterization of D2 Tool Steel fabricated thru Fused Filament Fabrication Process

Johanna Johnsson¹, Therese Tufvesson², José Costa³

¹Department of Supply chain and operation management, School of Engineering, Jönköping University; Gjuterigatan 5, 553 18 JÖNKÖPING, Sweden (jojo18af@student.ju.se)

²Department of Supply chain and operation management, School of Engineering, Jönköping University; Gjuterigatan 5, 553 18 JÖNKÖPING, Sweden (tuth18qe@student.ju.se)




³Department of Metallurgical and Materials Engineering, Faculdade de Engenharia, Universidade do Porto and LAETA/INEGI - Institute of Science and Innovation in Mechanical and Industrial Engineering, Rua Dr. Roberto Frias, 4200-465 PORTO, Portugal (jose.costa@fe.up.pt) ORCID [0000-0002-1714-4671](https://orcid.org/0000-0002-1714-4671)

Abstract

Additive Manufacturing (AM) unlocked a new way of producing more robust structures that use less material, enabling new possibilities due to design freedom, easiness of manufacturing complex parts, and mass personalization. One of the most common AM processes is Fused Filament Fabrication (FFF), used to manufacture polymer parts. However, FFF can produce metallic components, which are more complex and direct since it requires debinding and sintering processes. This study was conducted to develop the knowledge of FFF using metal and aims to evaluate the characteristics of D2 tool steel. The mechanical and microstructural properties were evaluated, and the results were compared with the supplier's datasheets.

Author Keywords. Additive Manufacturing; D2 Tool Steel; Material Extrusion; Fused Filament Fabrication; Metallic Materials Filaments, Feedstocks.

Type: Research Article

 Open Access  Peer Reviewed  CC BY

1. Introduction

Additive manufacturing (AM), commonly recognized as 3D printing, has recently gained enormous interest in the academic and industrial world (Costa et al. 2021). AM allows complex geometries to be produced layer-to-layer using powder, wire, or sheet as a feeding material into a high-energy heating source (Haghdadi et al. 2021). It brings versatility and flexibility and allows the disruption of conventional fabrication methods on personal and corporate levels (DeRoy et al. 2018; Frazier 2014; Herderick 2011).

The AM process starts with a 3D model being designed in computer-aided design (CAD) software and is usually saved as an STL (the acronym for Standard Tessellation Language) file. Afterward, specialist software will slice the 3D model into cross-section layers that the AM machine will then use to construct the 3D model, as seen in [Figure 1](#). Two additional steps are added if the metal FFF process: the first is after the finished fabrication process, the component will typically be lowered down into a wash chamber where the wax binder will dissolve and, the second, when the part has dried, it will be placed in a furnace for debinding and sintering, where the remaining binders will be removed, and the metal will be solidified.

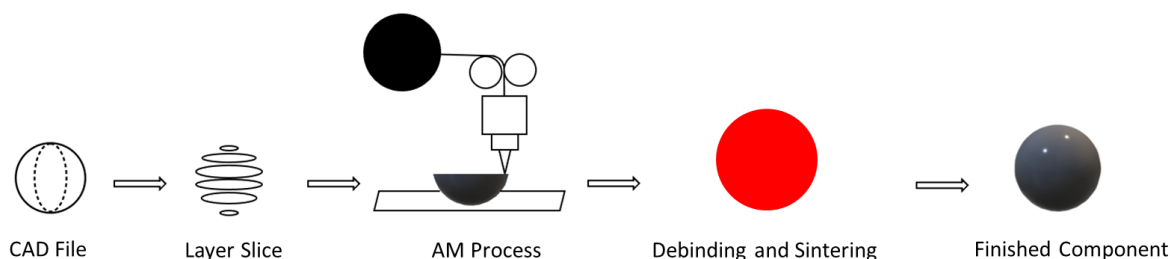


Figure 1: The FFF process for metallic materials

Since the start, AM technology has gone through three phases, prototype, end-use part, and production by the end-user. As indicated in the first phase, AM was only used to produce prototypes. Compared with the traditional way of producing prototypes, it reduced the time to market and enabled low-cost production. AM technology can also increase the security and privacy of companies and their R&D teams since it enables them to avoid sharing sensitive information with external suppliers or, if the equipment is available internally, produce prototypes without subcontracting. The manufacturers saw the opportunities and benefits AM had, and this is when the second phase started for end-use parts. Instead of taking days or weeks, it only takes a couple of hours in a small manufacturing space to produce complex and customized products; this step is commonly called "rapid tooling." The last phase was possible because low-cost 3D printers are available in the market; this enabled the end customer to buy and use AM by themselves (Costa et al. 2021; Mellor, Hao, and Zhang 2014). According to the ISO/ASTM52921-13 (ASTM 2019), FFF for metallic materials is a Solid-State Metal Additive Manufacturing method (Tuncer and Bose 2020) and is part of the category of Material Extrusion (MEX), where a filament is pushed through a heated nozzle. It was first developed for polymeric filaments but, nowadays, is used for metal if the filament is made of a polymeric binder system and metallic powder, where the mixture intends to disperse the metal powder in the binder (P. Singh et al. 2019; Costa et al. 2021; Sequeiros et al. 2020; G. Singh et al. 2021). The FFF roads are the filament strands located on the same layer, fused to create the essential mechanical properties. The fusion between the roads and layers creates anisotropic properties, with the weakest strength in the vertical axis and the highest strength in the transverse plane (sagittal and transverse axis)(Coogan and Kazmer 2020). With AM, there is now a possibility to end up with a high strength-to-weight ratio by simply putting material where the material is needed (Park et al. 2014).

This research will look at the FFF technology of the metallic filament of D2 tool steel. The microstructural and mechanical characterizations allow for comparing these materials' attributes to those of traditional materials, allowing for evaluating process efficiency.

2. Materials and method

The components were produced by FFF additive manufacturing technology, using standard and low-priced FFF equipment from Markforged. After production, the specimens went through the debinding and sintering process according to filament supplier conditions for D2 tool steel, which are not possible to disclose due to a non-disclosure agreement. The composition of D2 tool steel is shown in [Table 1](#).

Material Composition (%)	Cr	C	Mo	V	Ni+Cu	Mn	Si	P	S	Iron
D2 tool Steel	11~13	1.4~1.6	0.7~1.2	0.5~1.1	<0.75	0.1~0.6	0.1~0.6	<0.03	<0.03	bal.

Table 1: Material composition of D2 tool steel

Three different types of specimens were produced for the mechanical and microstructural characterization and are presented in Figure 2. From left to right is a pyramidal cube, used for hardness and microstructure characterization, tensile strength specimens, and dimensional.

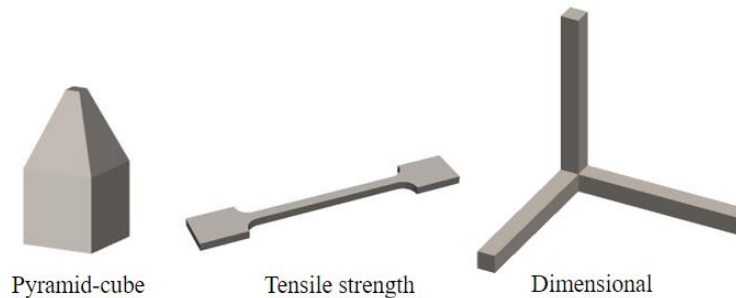


Figure 2: Specimens produced by FFF for the mechanical and microstructural characterization

The tests' preparation entailed first cutting the pyramidal cube in the transverse and longitudinal plane, then polishing the pieces to a mirror surface down to 1 μ diamond suspension. To see the microstructure of the D2 tool steel, the surface got etched with Nital 6%. Three types of pictures were taken on the microstructure, one from an optical microscope, another with a scanning electron microscope (SEM), and the last with energy-dispersive X-ray spectroscopy (EDS). The microscope used was FEG-ESEM / EDS / EBSD El Quanta 400FEG ESEM / EDAX Genesis X4M.

Pictures were taken with a Leica DVM6 microscope to evaluate roughness and dimensions. The pyramidal cube was used to evaluate the roughness, and the dimensional was used to evaluate the dimension accuracy. The software Las X was used to analyze the tests.

The tensile strength test was conducted according to NP EN 10002-1 standard with an EZ-SX Short Model. Five tests were performed.

The pyramidal cube went through heat treatment in a Termolab Furnace. First, the piece was heated slowly to 760 °C; then, the piece rested at 760 °C for 30 minutes. Then, it heated up to 1040 °C; when the temperature was stabilized, the specimen rested at 1040 °C for 30 minutes. When 30 minutes terminated, the specimen was taken out of the oven and placed on a ceramic plate to cool. At last, the specimen was put into the furnace at 200 °C for 30 minutes, then taken out to cool down, to then repeat the step one more time.

After the heat treatment, a Rockwell hardness C test with a 120° angle was performed on the specimen "pyramid-cube." All tests were made on the same surface, but the location was changed for each test. To perform the test, Emcotest DuraVisison G5 was used.

3. Result and discussion

The standard mechanical properties of filament suppliers are presented in Table 2 for the following states: as-sintered, heat treated and wrought.

Typical Mechanical Properties	Standard	As-Sintered	Heat-Treated	Wrought Heat Treated
0.2% Compressive Yield Strength	ASTM E9	830 MPa	1 690 MPa	2 200 MPa
Elastic Modulus	ASTM E9	170 GPa	187 GPa	210 GPa
Hardness	ASTM E18	54 HRC	55 HRC	62 HRC
Relative Density	ASTM B923	97 %	97%	100%

Table 2: Mechanical properties for D2 Tool Steel

3.1. Scanning Electron Microscopy (SEM) analysis

The filament of D2 tool steel and the longitude and transverse plane of the produced pyramidal cube was analyzed by SEM.

3.1.1. Filament

The D2 filament surface was observed in SEM before the FFF process, as seen in Figure 3 (a). The EDS surface analysis the picture (c), from the light big grain in the picture (b), shows the weight percentage of the grain. The EDS scan in picture (c) shows that the large grains mainly consist of Iron (Fe) and a lower percentage of Chromium (Cr) and Vanadium (V). The weight percentage compared with the datasheet of D2 tool steel in Table 1 shows it is in the range.

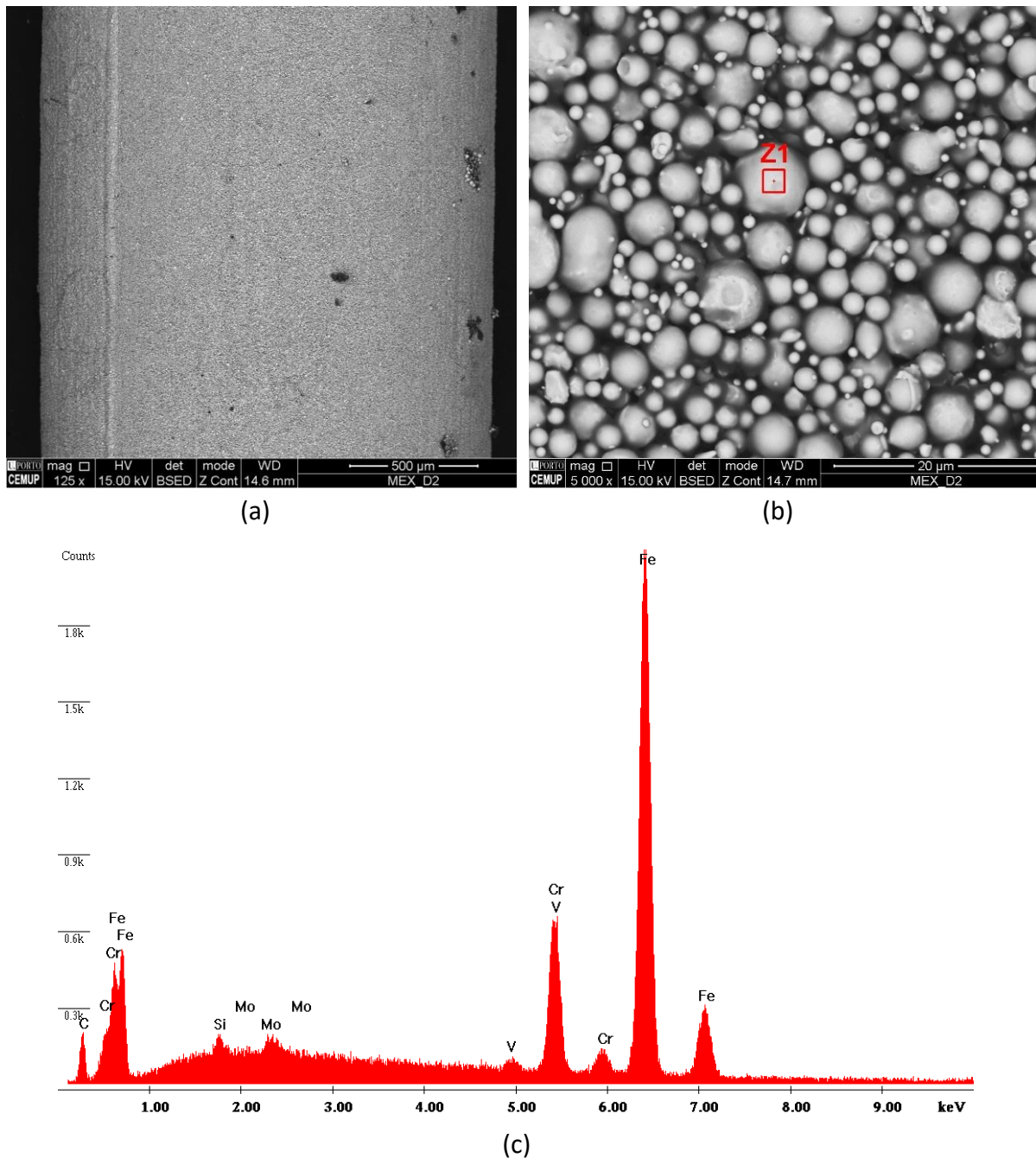


Figure 3: (a) and (b) SEM pictures of D2 tool steel filament with different magnifications, (c) EDS surface analysis of Z1 in (b).

3.1.2. Longitude

The air gaps between the filament in [Figure 4 \(a\)](#) show that the specimen is not 100% dense. In addition, in [Figure 4 \(b\)](#), oxides show, according to [Table 2](#), D2 tool steel should be 97% dense.

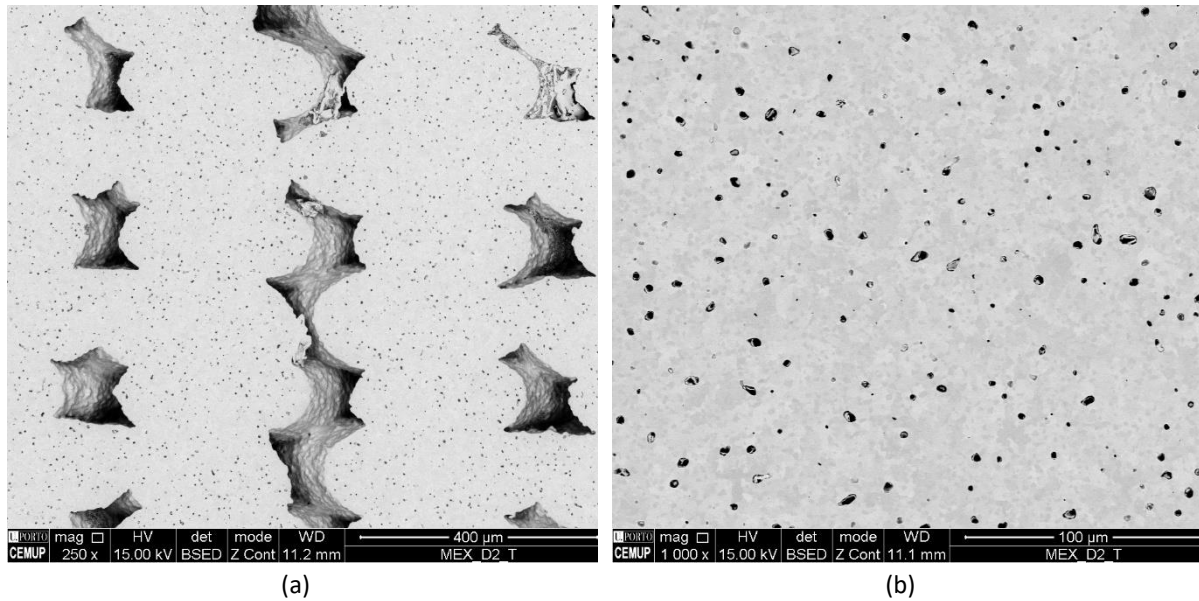
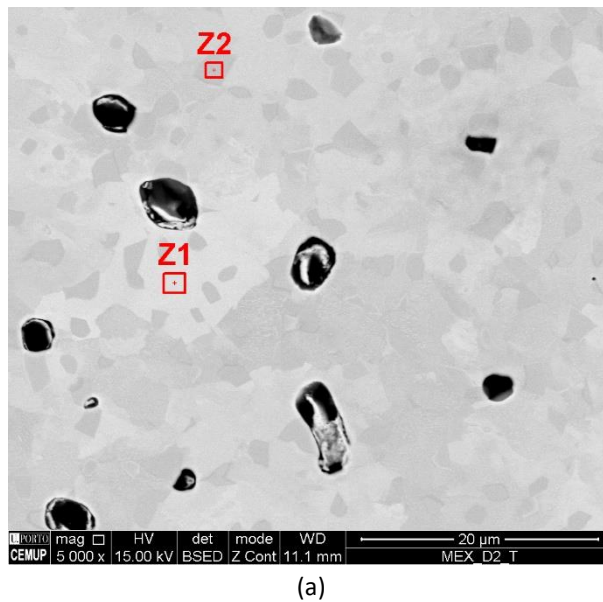
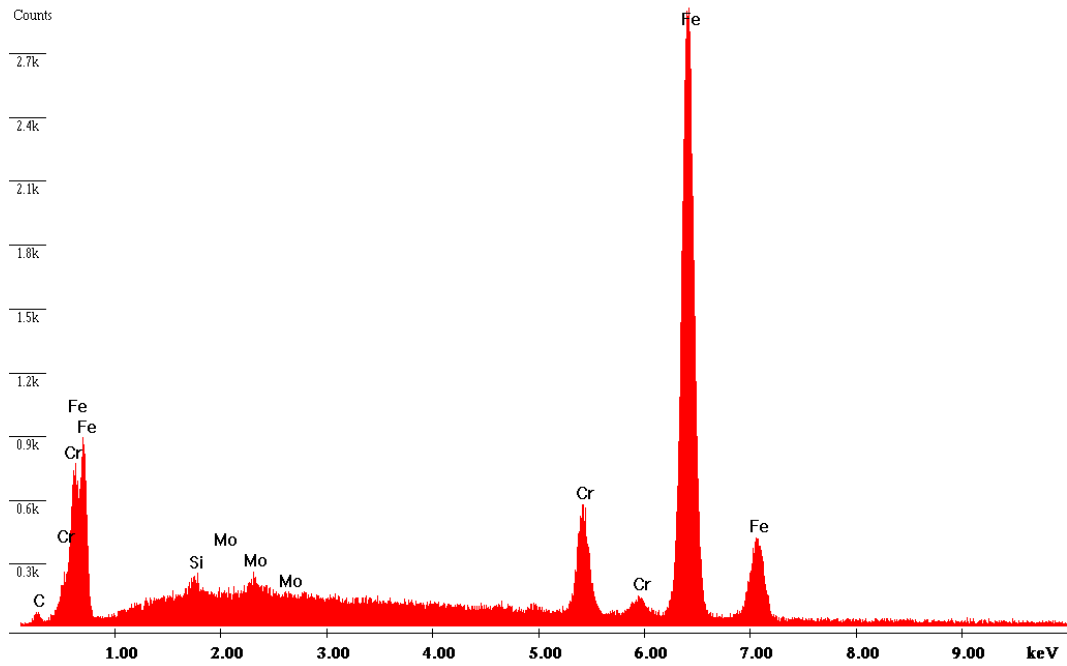


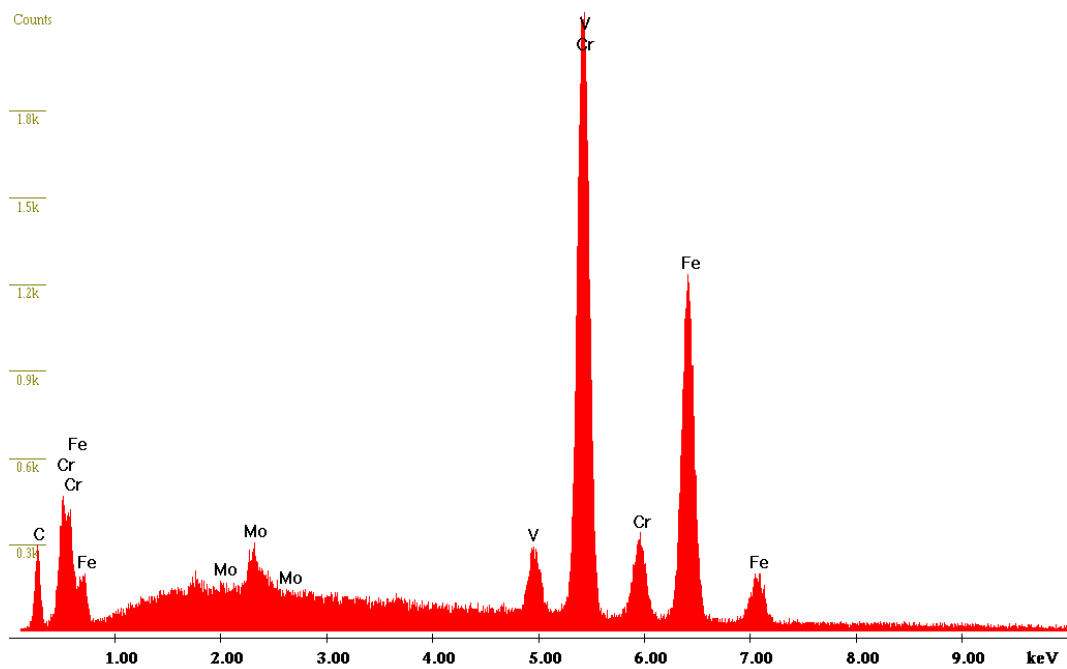
Figure 4: Different magnifications of the longitude cut.

The EDS analysis of Z1 is available in [Figure 5 \(b\)](#), where the lighter part in (a) is not comparable with the material composition of D2 tool steel in [Table 2](#). The same conclusion for Z2 in the darker grains, [Figure 5 \(c\)](#).





(b)



(c)

Figure 5: EDS analysis of light grey and dark grey zone.

3.1.3. Transverse

Figure 6 (a) and (b) displays problem in the specimen, such as cracks and big voids (air gaps) between the filament strings.

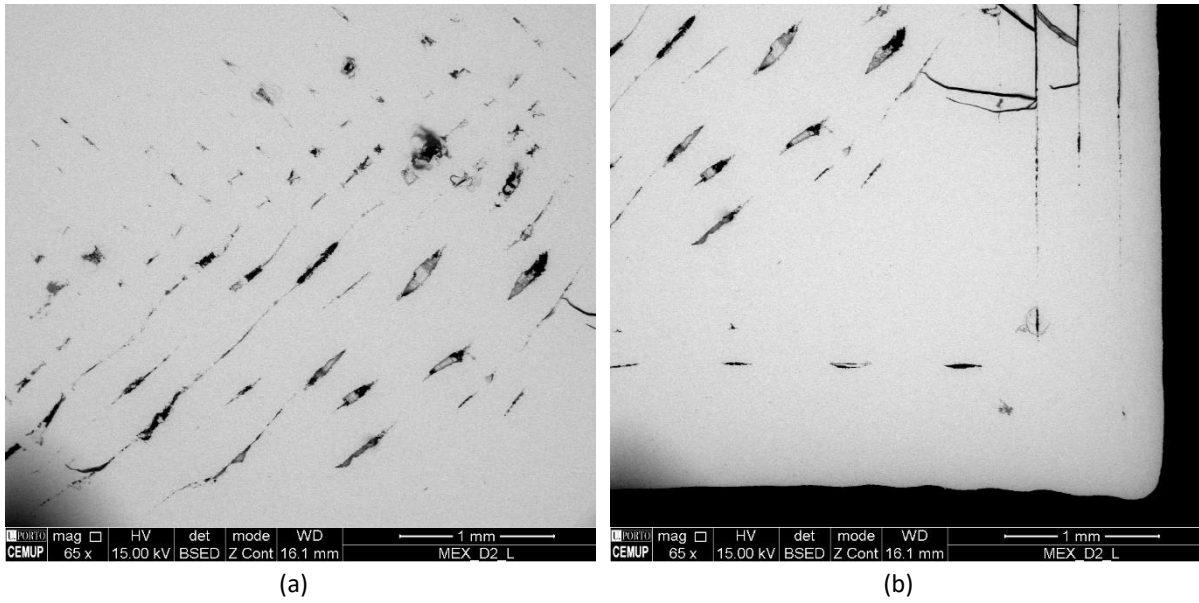
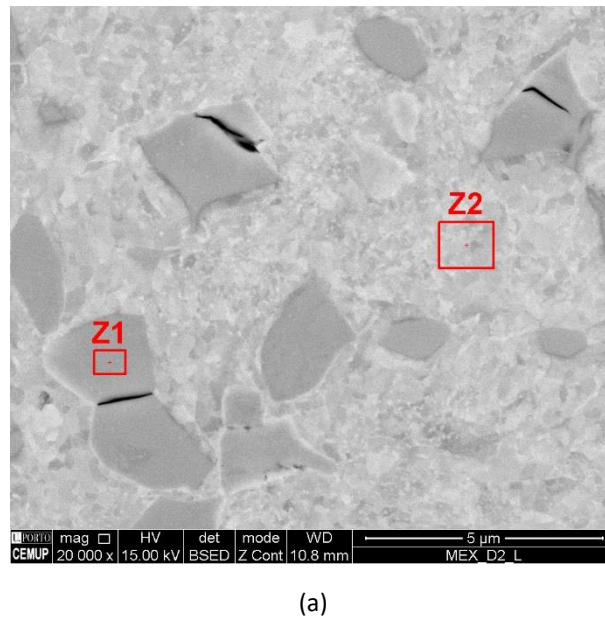
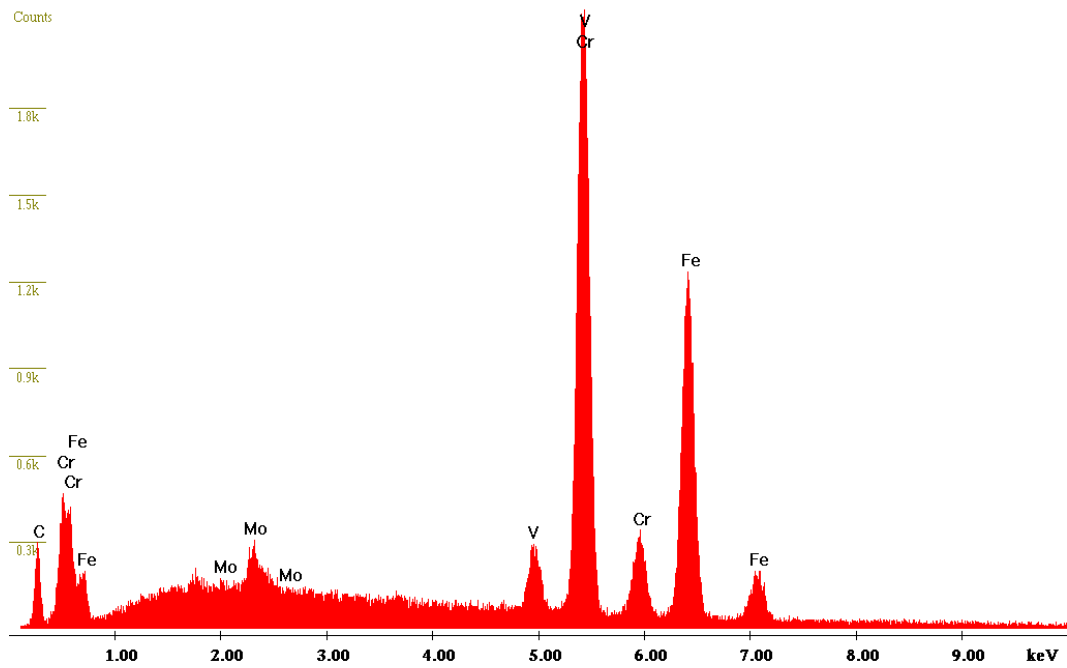


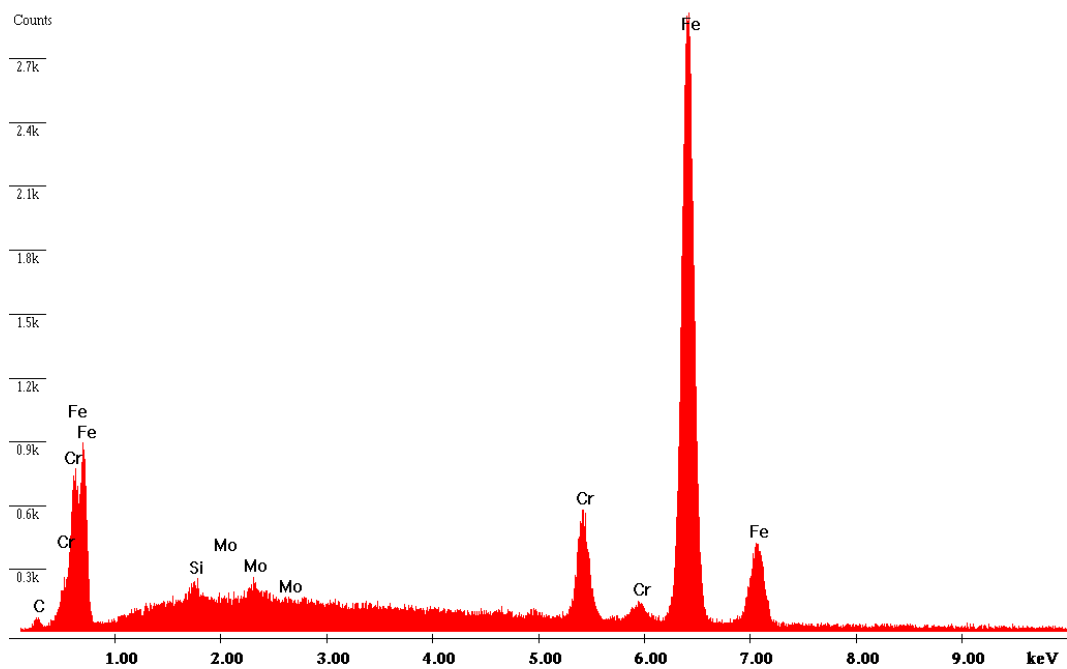
Figure 6: Problems in the specimen.

Similar result to the cut in the longitude plane, with a higher percentage of iron in the light zone area (Z2), and a higher percentage of chromium in the dark spots, as shown. In [Figure 7](#) (a), the cracks appear only on the dark grey spots; the darker seen, the harder the material is, and the more brittle it is.





(b)



(c)

Figure 7: (a) cracks in the dark grain, (b) and (c) EDS analysis of the big dark grain and the lighter zone.

In [Table 3](#), a summary of the weight percentage from each EDS scan is shown. The scan of the light grains in transverse and longitude cuts shows that they have similar composition, and the dark grains in the two cuts also had a comparable composition. The composition of dark grain together with light areas, but with a higher ratio of light, is probably more similar to the actual weight percentage of the material.

Element Weight %	Cr	C	Mo	V	Ni + Cu	Mn	S	P	S	Iron%
Z1	13.08		1.03	0.97			0.57			84.35
Z1-L-Light	7.16	1.02	0.97				0.62			90.23
Z2-T-Light	7.52	0.89	1.31				0.54			89.74
Z1-T-Dark	44.14	4.69	2.48	4.16						44.52
Z2-L-Dark	44.78	4.3	2.43	4.55						43.94

Table 3: Weight percentage from each EDS scan

3.2. Microstructure observations

After comparing the microstructure with the one available in the article *Effect of high-temperature heating on chemical changes in M7C3 carbides of AISI D2 tool steel* (Nykiel and Hryniewicz 2014), the microstructure of D2 tool steel can be determined to be martensite and seen in Figure 8.

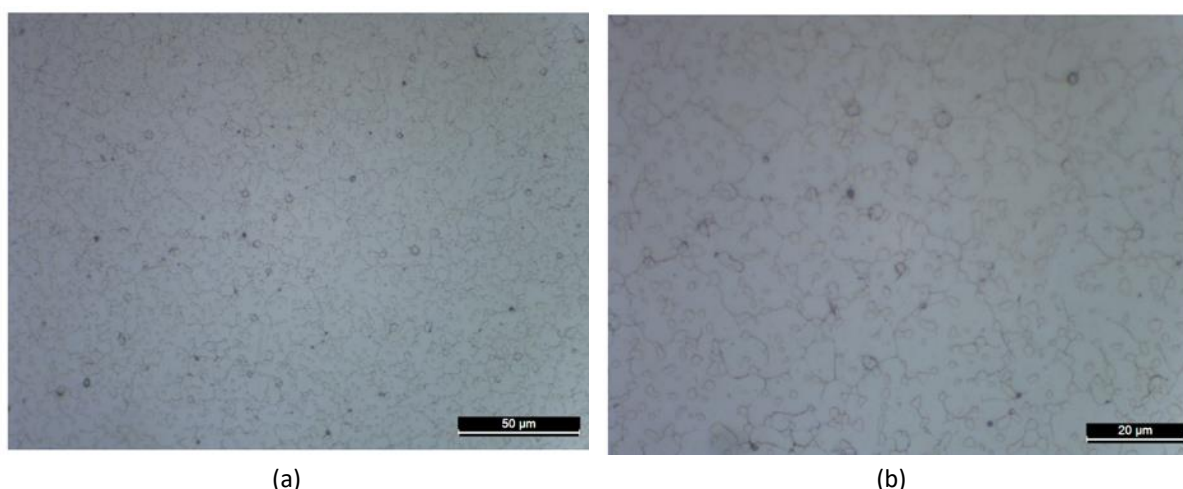


Figure 8: Heat-treated D2 tool steel etched with 6% Nital. (a) Magnifying lens 50x. (b) magnifying lens 100x.

3.3. Mechanical characterization

3.3.1. Tensile test

Regarding the tensile test, four of the five specimens fractured at the bottom, and the data merely provided the yield strength of two of them (Table 4). Both yield strength values were under the reference value of 830 MPa supplied by the material supplier in (Table 2), which decreased between 8% and 11%.

	Specimen 1	Specimen 2	Specimen 3	Specimen 4	Specimen 5
Ultimate Stress [MPa_{max}]	1215.18	1199.44	1126.52	1195.64	1074.51
Yield strength [MPa]			740		760

Table 4: Ultimate stress of D2 tool steel.

Some factors might be able to justify this. First, it might be due to poor adhesion between the layers, as seen in Figure 4 and 5, which is reinforced by the debonding and sintering process. This could be solved by introducing a feature to prevent slipping from occurring. Secondly, the debinding and sintering processes might have been poorly performed, increasing the material's porosity. Thirdly, during the testing, the specimens were exposed to sliding. All these factors may have been affected individually or together. Regarding the specimens fracturing at the bottom, the ductility must have been higher than the values recorded. This is due to the deformation located outside the region being measured.

3.3.2. Hardness test

The hardness test result did not match the reference value provided in the datasheet (Table 3). The mean value of the test was approximately 44 HRC, which is 11 HRC below the reference value (Figure 9 Figure 1). The standard deviation value of D2 tool steel was 1 HRC.

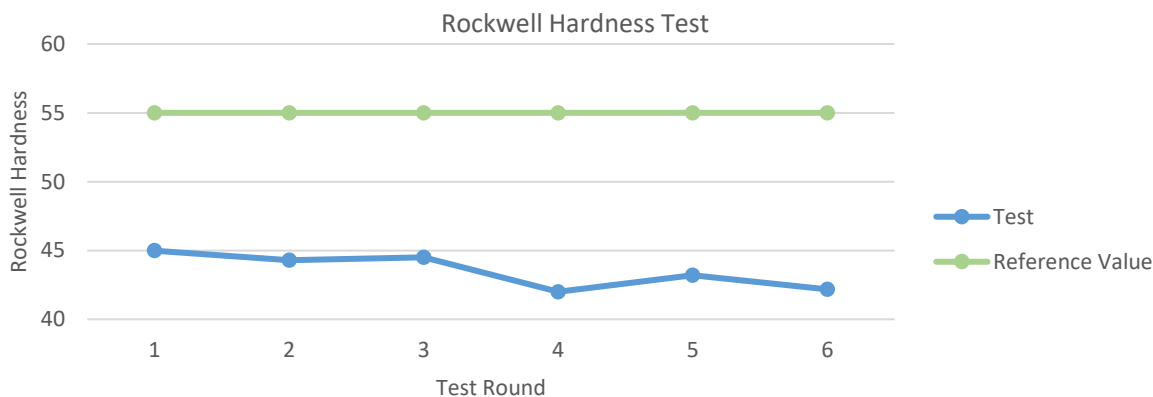


Figure 9: Rockwell hardness test on D2 tool steel.

The reason for the hardness being 21 % under the reference value can be due to the poor adhesion between the layers, which can be seen in Figure 4 and 6. It might also have been due to errors that might have occurred during the tempering process in the furnace.

3.3.3. Roughness

In Figure 10, three lines (a), (b) and (c) were evaluated for their amplitude and material ratio parameters. (c) is following the line the filament string got printed, while (a) and (b) are perpendicular to (c).

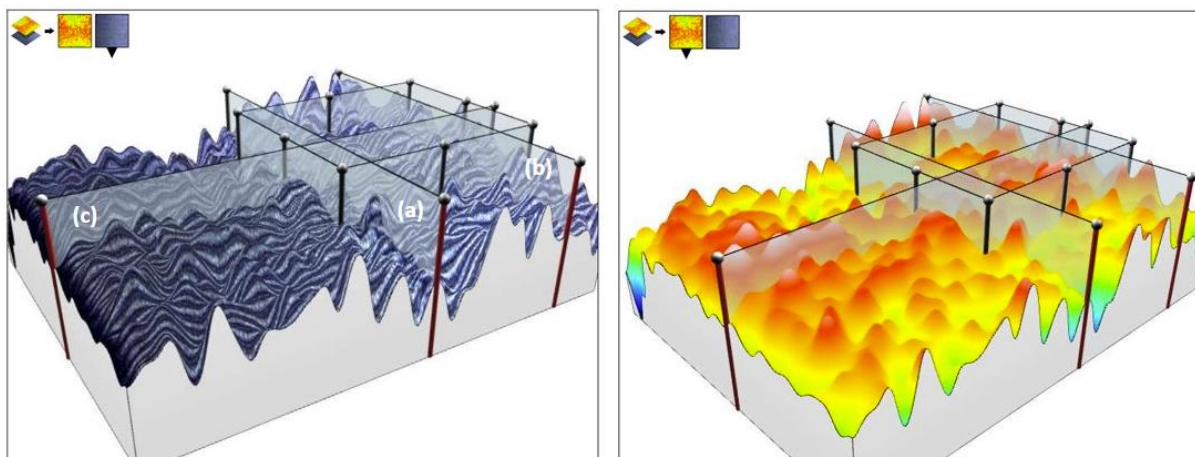


Figure 10: Picture of the Topography layer.

In Figure 11, the roughness of the different lines (a), (b), and (c) is shown. The R_a (average roughness) values for each line are shown in Table 5; compared with typical R_a values for engineering surfaces corresponding to sawing, planing, and forging. The roughness from AM technology is on the rough side of the different surfaces. R_{sk} (Skewness value) describes how the surface is distributed around the mean line. if $R_{sk} > 0$, typically, the tribological surface is bad. If the top of the curve is located on the negative side. $R_{sk} < 0$. the surface is better because it is flatter at the top, and the top of the curve is located on the positive side of the mean line. Hence (b) in Table 5 Table 5 have a better surface because it is negative. while the other two lines (a) and (c) are worse. The R_{ku} . is a measure in sharpness in

profile peak. If R_{ku} is smaller than 3, it indicates that the probability is smaller of finding the profile at the mean line. Pictures were taken with a Leica DVM6 microscope to evaluate roughness and dimensions and there is a higher chance of finding it of the mean line. If R_{ku} is larger. It means that the probability of finding the profile at the mean line is higher than finding it at the mean line. Each of the lines (a), (b), and (c) are below 3, which is good.

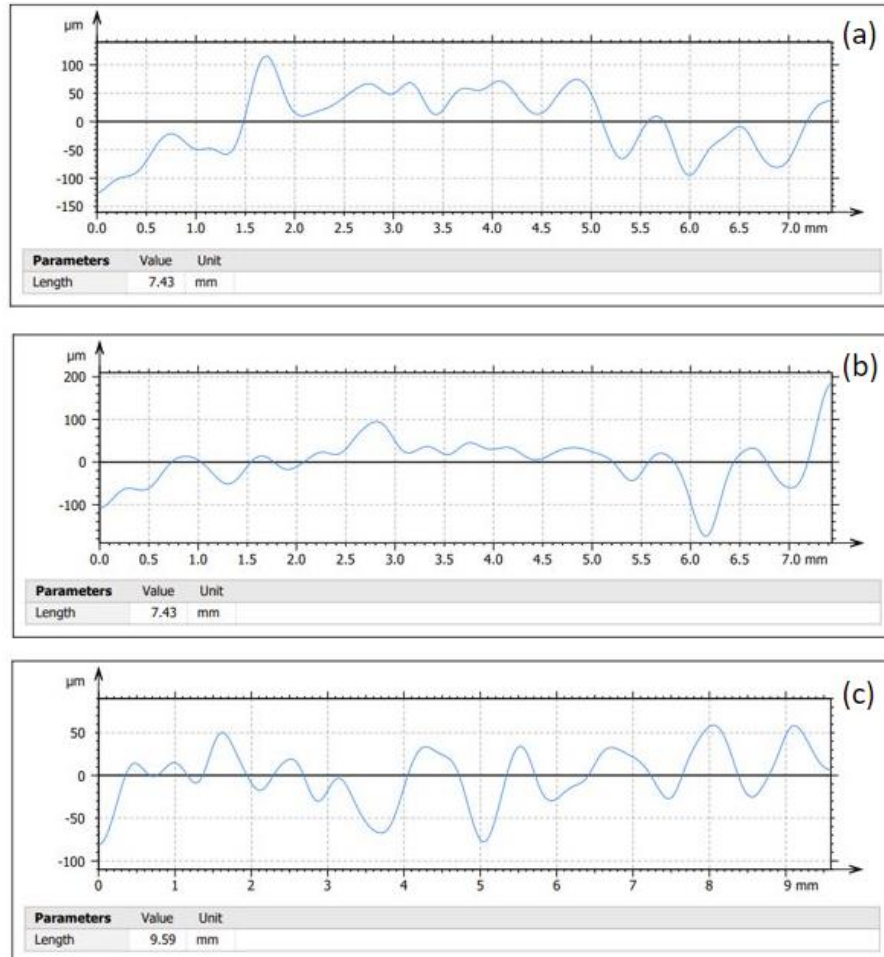


Figure 11: Roughness of the different test lines

		Parameters	Sample (a)	Sample (b)	Sample (c)
Amplitude	R_p (μm)		22.2	17.5	13.3
	R_v (μm)		19.7	22.3	11.8
	R_z (μm)		41.9	39.7	25.1
	R_c (μm)	No averaging (single value)	35.7	31.1	26.8
	R_t (μm)		72.1	85.9	40.9
	R_a (μm)		11.0	12.0	7.53
	R_q (μm)		13.2	13.5	8.56
	R_{sk}		0.0628	-0.103	0.0204
	R_{ku}		2.17	1.85	1.78
Material ratio	R_{mr} (%)	$c = 1 \mu\text{m}$ below highest peak	0.622	2.22	0.945
	R_{dc} (μm)	$p = 20\%$ $q=80\%$	23.5	22.0	17.3

Table 5: Roughness parameters

3.3.4. Dimensional analyses

In Figure 12 the dimensions of the dimensional specimen can be seen after the sintering process. The angle of 90° is no longer accurate, and the same is true for three out of the four

measurements that were taken. The increase, going from the top measurement in a counterclockwise motion, is 0%, 9%, 0.7%, and 1.3%.

It is interesting to note that the length and width of the material increased while the angle decreased. The increase might be a miscalculation of the AM machine when it is compensated with the material due to the shrinking processes that occur after sintering. It might also be due to a poorly performed debinding and sintering process, resulting in residue of the polymer binder remaining in the sample. Another explanation could be the poor adhesion between the layers, resulting in more significant dimensions.

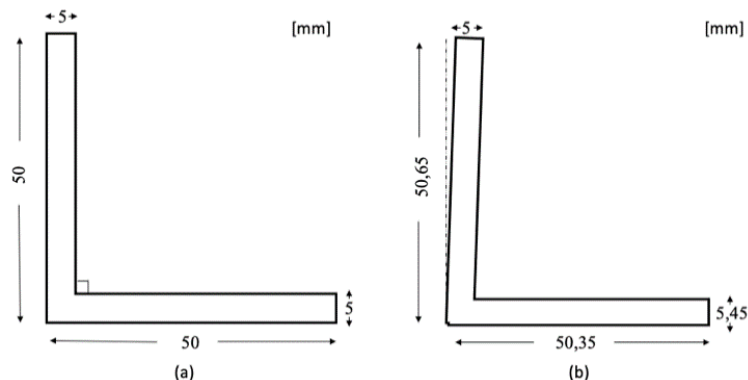


Figure 12: Dimension of Dimensional specimen. (a) reference dimensions. (b) actual dimensions.

4. Conclusion

This research aimed to identify the characteristics of D2 tool steel after being manufactured in a ME AM process.

The results of the various tests did not match the datasheet from the suppliers. The hardness and tensile test of D2 tool steel were below the reference values, and the dimensions were not accurate either. In conclusion, D2 tool steel has the potential to improve and achieve better results.

A suggestion for future work is to redo the test with other settings to minimize the risk of under extrusion. Furthermore, it is suggested to mark the tensile strength specimens to show how they were printed to see if they all will break in the same place. A recommendation to the suppliers is to update their datasheets more frequently since every third year is not enough.

References

- Coogan, Timothy J, and David O Kazmer. 2020. "Prediction of Interlayer Strength in Material Extrusion Additive Manufacturing." *Additive Manufacturing* 35 (October): 101368. <https://doi.org/10.1016/j.addma.2020.101368>.
- Costa, José, Elsa Sequeiros, Maria Teresa Vieira, and Manuel Vieira. 2021. "Additive Manufacturing: Material Extrusion of Metallic Parts." *U.Porto Journal of Engineering* 7 (3): 53–69. https://doi.org/10.24840/2183-6493_007.003_0005.
- DebRoy, T., H.L. Wei, J.S. Zuback, T. Mukherjee, J.W. Elmer, J.O. Milewski, A.M. Beese, A. Wilson-Heid, A. De, and W. Zhang. 2018. "Additive Manufacturing of Metallic Components – Process, Structure and Properties." *Progress in Materials Science* 92 (March): 112–224. <https://doi.org/10.1016/j.pmatsci.2017.10.001>.

- F42 Committee. 2019. "Standard Terminology for Additive Manufacturing—Coordinate Systems and Test Methodologies." ASTM52921-13(2019). ASTM International. <https://doi.org/10.1520/ISOASTM52921-13R19>.
- Frazier, William E. 2014. "Metal Additive Manufacturing: A Review." *Journal of Materials Engineering and Performance* 23 (6): 1917–28. <https://doi.org/10.1007/s11665-014-0958-z>.
- Haghdadi, Nima, Majid Laleh, Maxwell Moyle, and Sophie Primig. 2021. "Additive Manufacturing of Steels: A Review of Achievements and Challenges." *Journal of Materials Science* 56 (1): 64–107. <https://doi.org/10.1007/s10853-020-05109-0>.
- Herderick, E. 2011. "Additive Manufacturing of Metals: A Review." In . Columbus, Ohio. <https://www.asminternational.org/documents/10192/23826899/cp2011mstp1413.pdf/04f142d0-f1ca-44d4-8a10-891992e5529a>.
- Mellor, Stephen, Liang Hao, and David Zhang. 2014. "Additive Manufacturing: A Framework for Implementation." *International Journal of Production Economics* 149 (March): 194–201. <https://doi.org/10.1016/j.ijpe.2013.07.008>.
- Nykiel, Tadeusz, and Tadeusz Hryniewicz. 2014. "Effect of High-Temperature Heating on Chemical Changes in M7C3 Carbides of AISI D2 Tool Steel." *International Letters of Chemistry, Physics and Astronomy* 36 (July): 258–71. <https://doi.org/10.56431/p-6203wy>.
- Park, Sang-In, David W. Rosen, Seung-kyum Choi, and Chad E. Duty. 2014. "Effective Mechanical Properties of Lattice Material Fabricated by Material Extrusion Additive Manufacturing." *Additive Manufacturing* 1–4 (October): 12–23. <https://doi.org/10.1016/j.addma.2014.07.002>.
- Sequeiros, Elsa W., Omid Emadnia, Maria Teresa Vieira, and Manuel Fernando Vieira. 2020. "Development of Metal Powder Hot Embossing: A New Method for Micromanufacturing." *Metals* 10 (3): 388. <https://doi.org/10.3390/met10030388>.
- Singh, Gurminder, Jean-Michel Missiaen, Didier Bouvard, and Jean-Marc Chaix. 2021. "Additive Manufacturing of 17–4 PH Steel Using Metal Injection Molding Feedstock: Analysis of 3D Extrusion Printing, Debinding and Sintering." *Additive Manufacturing* 47 (November): 102287. <https://doi.org/10.1016/j.addma.2021.102287>.
- Singh, Paramjot, Qasim Shaikh, Vamsi K. Balla, Sundar V. Atre, and Kunal H. Kate. 2020. "Estimating Powder-Polymer Material Properties Used in Design for Metal Fused Filament Fabrication (DfMF3)." *JOM* 72 (1): 485–95. <https://doi.org/10.1007/s11837-019-03920-y>.
- Tuncer, Nihan, and Animesh Bose. 2020. "Solid-State Metal Additive Manufacturing: A Review." *JOM* 72 (9): 3090–3111. <https://doi.org/10.1007/s11837-020-04260-y>.